Robust DC-Link Control in EVs With Multiple Energy Storage Systems

Ricardo de Castro, *Student Member, IEEE*, Rui Esteves Araújo, *Member, IEEE*, João Pedro F. Trovão, *Student Member, IEEE*, Paulo G. Pereirinha, *Member, IEEE*, Pedro Melo, *Student Member, IEEE*, and Diamantino Freitas

***Abstract*—The energy storage system (ESS), as well as its efficient management, represents a key factor for the success of electric vehicles. Due to well-known technological constraints in ESSs, there has been a growing interest in combining various types of energy sources with complementary features. Among the many possible combinations, our interest here lies in the hybridization of batteries and supercapacitors (SCs) with an active parallel arrangement, i.e., the sources are connected to the direct current (dc) bus through two bidirectional dc–dc converters (step-up). Based on this ESS topology, a robust dc-link controller is employed to regulate the dc-bus voltage and track the SCs current in spite of uncertainties in the system. For this purpose, we start by showing that the converters' uncertainty, e.g., the powertrain load, can be modeled as a convex polytope. The dc-link controller is then posed as a robust linear-quadratic regulator problem and, by exploring the convex polytope, converted in a linear matrix inequalities framework, which can efficiently be solved by numerical means. Finally, the operation envelope of the controller is extended by scheduling the gains according to the energy sources' voltages, which is an important feature to cope with the voltage variations in the SCs. To analyze the performance of the control architecture, a reduced-scale prototype was built. The experimental results show that, compared with the nonrobust and non-gain-scheduled controllers, the proposed dc-link controller offers better transient response and robustness to disturbances. Furthermore, the global performance of the controller is evaluated during certain driving cycles.**

***Index Terms*—Batteries, dc–dc power converters, electric vehicles (EVs), load flow control, robust control, supercapacitors (SCs).**

Manuscript received December 20, 2011; revised April 17, 2012; accepted June 11, 2012. Date of publication July 17, 2012; date of current version October 12, 2012. This work was supported in part by the Science and Technology Foundation under Grant SFRH/BD/47882/2008, Grant SFRH/BD/36094/2007, project Grant PTDC/EEA-EEL/121284/2010 and FCOMP-01-0124-FEDER-020391. The review of this paper was coordinated by Prof. M. E. Benbouzid.

R. de Castro and D. Freitas are with the Department of Electrical and Computer Engineering, Faculty of Engineering, University of Porto, 4200-465 Porto, Portugal (e-mail: de.castro@fe.up.pt; dfreitas@fe.up.pt).

R. E. Araújo is with the INESC TEC (formerly INESC Porto) and Faculty of Engineering, University of Porto, 4200-465 Porto, Portugal (e-mail: raraujo@fe.up.pt).

J. P. F. Trovão and P. G. Pereirinha are with the Department of Electrical Engineering, Polytechnic Institute of Coimbra–Coimbra Institute of Engineering, 3030-199 Coimbra, Portugal, and also with the Institute for Systems and Computers Engineering at Coimbra, 3000-033 Coimbra, Portugal (e-mail: jtrovao@isec.pt; ppereiri@isec.pt).

P. Melo is with the Department of Electrical Engineering, School of Engineering, Polytechnic Institute of Porto, 4200-072 Porto, Portugal (e-mail: pma@isep.ipp.pt).

Color versions of one or more of the figures in this paper are available online at http://ieeexplore.ieee.org.

Digital Object Identifier 10.1109/TVT.2012.2208772

I. Introduction

THE FUTURE of sustainable mobility is closely tied to the development of electric vehicles (EVs). Indeed, EVs are much more silent, cleaner, and more energy efficient, both from a local and global point of view, than vehicles that are based on the internal combustion engine [1]. Recently, there have been great advances on the energy density, power density, life cycles, safety, and cost of energy storage systems (ESSs) [2]–[4]. Despite these efforts, an affordable ESS with both high energy and high power density is not yet available [5]. These factors have motivated the development of hybrid ESSs, which are composed of multiple energy sources with complementary features. For example, high energy density is an important feature for satisfying the EV range requirements, which can be provided by batteries. On the other hand, to meet the EV acceleration and regenerative breaking demands, which are typical of urban conditions, high-specific-power devices with fast responses are more convenient, e.g., supercapacitors (SCs) [4], [6]–[9]. Consequently, this paper addresses the hybridization of ESS with batteries and SCs, focusing on the robust control of the power converters that are employed to manage the energy flow between the sources and loads.

An overview of the main topologies used to hybridize the ESS are presented and discussed in [2]. From a cost point of view, using a single converter is the most advantageous solution, e.g., fixing the dc-link voltage with the battery and employing a converter to regulate the SC power [7], [8], [10], [11]. From a practical perspective, however, this configuration is not always possible, because the battery pack voltage may not match the motor inverter ratings. Because of this issue, there has been an increasing interest in the development of parallel active battery/SC topologies [4], [12]–[14]. In this paper, we consider that the battery pack and the SCs are connected, in parallel, to the dc-link through two boost converters. Although the use of two dc–dc converters increases the cost and size, this topology allows us to have a separate control over the power flow of each source, which is a valuable feature for the ESS hybridization.

Two fundamental issues must be considered when implementing the aforementioned hybrid ESS. First, we must decide how to split, throughout the EV mission, the power among the sources. Second, to impose these power/current set points, a suitable control strategy for the converters' duty cycles must be devised. Although both issues can be handled in an integrated way (for example, see [15]), in this paper, we advocate a two-layer separation, as illustrated in Fig. 1. Accordingly, the top

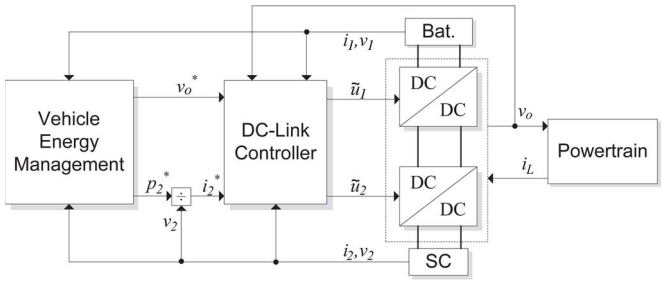

Fig. 1. Generic architecture of the hybrid ESS with batteries and SCs. Variables with subscript 1 refer to the primary source, i.e., batteries, whereas subscript 2 is employed in the secondary source, i.e., the SCs.

layer, called vehicle energy management (VEM), in addition to the power allocation duties, can also set the desired voltage level for the dc bus. The typical framework in the VEM consists of an optimization problem that aims at minimizing, over a mission, the energy losses of the hybrid ESS, subject to a set of constraints such as the state-of-charge (SOC) dynamics, input/output power balance, and ESS physical limits [15]. Subsequently, the optimum power division can be obtained using numerical techniques such as dynamic programming [16] or by analytical means [17]. Although this methodology can find the optimal allocation, its real-time implementation is hampered by the need to know, in advance, the vehicle driving cycle, which, in most cases, is difficult to predict. Thus, to overcome these obstacles, a growing interest has emerged in suboptimal but causal techniques such as stochastic optimization [18], machine learning [19], and several types of heuristics [10], [15], [20]. Although of pivotal importance, the VEM layer is not treated here, and in the following discussion, our concern will lie only on the second layer, i.e., the dc-link controller.

The dc-link controller has the responsibility of manipulating the converters' duty cycles so that the dc-bus voltage and the current (or power) of the auxiliary source, the SCs, follow the set points requested by the VEM (see Fig. 1). Assuming that the control of the dc-bus voltage and SC current are independent of each other, the control problem can be simplified using linear control techniques. For example, [8] and [13] report a design where linear proportional+integrals (PIs) are employed to build a dc-link controller based on the following two parallel loops: 1) a current loop for regulating the auxiliary current (SCs in this paper) and 2) a voltage–current (cascade) loop for, through the main source, keeping a constant output voltage. The main drawback of this approach is the fact that the voltage–current loop is not completely independent of the auxiliary current, e.g., a change in the current of the auxiliary source (SCs) affects the dc-bus voltage, which can lead to undesirable interaction between the loops. To attenuate this issue, [21] proposed a simple decoupling concept that compensates for the voltage–current controller for set point modifications in the auxiliary source. However, this decoupling relies on a power balance principle that is only valid in steady-state conditions. Another popular approach in the power electronics community is to linearize the (nonlinear) dc–dc converter model around an operating point and then design the feedback controller to locally stabilize the system [22]. For the hybrid ESS case, the main challenge is to ensure stability and good transient performance, in spite of disturbances, such as the powertrain loads (e.g., accelerating and regenerative braking present very different operation modes) and input voltages (e.g., typically, throughout the EV operation, the SC voltage displays variations of up to 50% of its nominal value). Consequently, to cope with all this uncertainty, it is necessary to endow the feedback controller with robust control techniques.

The main goal of this paper is to develop and evaluate a robust dc-link controller for hybrid ESSs composed of batteries and SCs, which are connected through the parallel of two step-up converters (see Fig. 1). In the power electronics literature, the robust control of dc–dc converters with the single-input–single-output structure has extensively been studied in recent years, particularly the boost and buck–boost topologies (for example, see [23]–[26]). Spurred by the dc-link control problem, these previous studies are extended here for the multiple-input–multiple-output (MIMO) structure, with particular emphasis on the configuration where two boost converters must operate in parallel and satisfy several control objectives (e.g. regulate the converter's output voltage and SCs' current). Toward that end, a robust linear-quadratic regulator (LQR) is proposed and then numerically solved within a linear matrix inequalities (LMI) framework. Besides the robustness property, the controller features an extended operation envelope due to the gain scheduling of the energy source voltages, which is particularly helpful in coping with voltage variations in SCs. Experimental validation of the control architecture is carried out in a reduced-scale hybrid ESS, and its advantages against nonrobust and non-gain-scheduled controllers is investigated.

The remainder of this paper is organized as follows. Section II presents the power converter model and a convenient state-space normalization. The robust dc-link controller is then discussed in Section III and experimentally validated, through a reduced-scale test bench, in Section IV. Finally, Section V provides the concluding remarks.

II. Model of the Power Converters

As depicted in Fig. 2, the topology used for the hybrid ESS is composed of two bidirectional boost dc–dc converters that are connected in parallel. These converters are supplied by two sources, a primary (the battery) and a secondary (the SCs), and have the responsibility of stepping up the input voltages to the dc-link levels, simultaneously providing an adequate bidirectional energy flow between the sources and the loads. As a starting point for the analysis of this system, the average model of the power converters [22], [27] is outlined as

$$L_1 \frac{di_1}{dt} = v_1 - v_o(1-\tilde{u}_1) \tag{1a}$$

$$L_2 \frac{di_2}{dt} = v_2 - v_o(1-\tilde{u}_2) \tag{1b}$$

$$C \frac{dv_o}{dt} = i_1(1-\tilde{u}_1) + i_2(1-\tilde{u}_2) - \frac{v_o}{R} - i_L \tag{1c}$$

where i_1, i_2 are the inductors' (average) currents, and v_o is the output (average) dc-link voltage. The two control inputs are the converters' duty cycles $(\tilde{u}_1, \tilde{u}_2) \in [0,1] \times [0,1]$. The

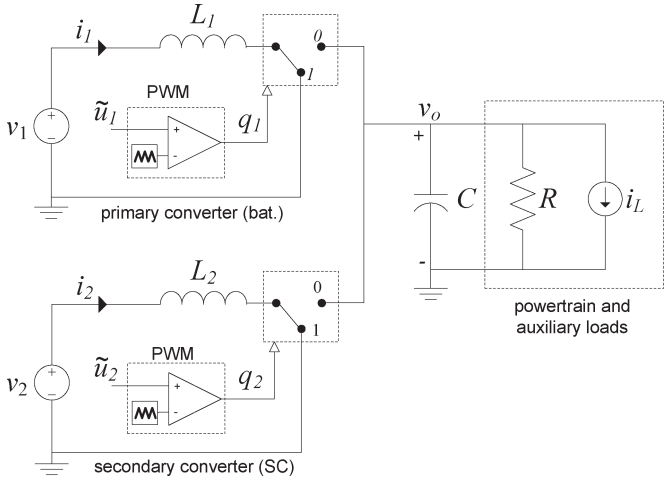

Fig. 2. Equivalent circuit of the dc–dc power converters employed in the hybrid ESS.

model parameters are given as follows: L_1, L_2 represent the converter inductances, C is the output capacitance, and R is the nominal resistance associated with the vehicle auxiliary loads. The exogenous inputs are represented by the battery (v_1) and SC (v_2) voltage and by the bounded load current $i_L \in [\underline{i_L}, \overline{i_L}]$ that models the vehicle power requests, which is positive during accelerations and negative when regenerative braking is applied. For mathematical convenience, i_L may also incorporate variations into the load of the auxiliary systems. With regard to the notation employed in the aforementioned model, the variables with subscript 1 are related to the primary source (the batteries), whereas subscript 2 refers to the secondary energy source (the SCs). Furthermore, throughout this paper, unless otherwise stated, we will refer to the minimum and maximum values that a given variable can take with an underline and overline notation (e.g., $\underline{i_L}$, $\overline{i_L}$), respectively.

In practice, the duty cycles $(\tilde{u}_1, \tilde{u}_2)$ are used by the pulsewidth modulator (PWM) block to generate the discrete gating signals $(q_1, q_2) \in \{0,1\} \times \{0,1\}$ and switch the power semiconductors, as illustrated in Fig. 2. With the aim of simplifying the analysis, the aforementioned model assumes ideal switches, neglects parasite elements in the inductances and capacitors, and, in general, can capture the converters' dynamics up to 1/10 the switching frequency [27], which is enough for the controller design.

A. Normalized Average Model

To facilitate the controller design, consider the following state normalization and time-scale transformation:

$$\begin{bmatrix} x_1 \\ x_2 \\ x_3 \end{bmatrix} = \begin{bmatrix} \frac{1}{v_1}\sqrt{\frac{L_1}{C}} & 0 & 0 \\ 0 & \frac{1}{v_2}\sqrt{\frac{L_1}{C}} & 0 \\ 0 & 0 & \frac{1}{v_1} \end{bmatrix} \begin{bmatrix} i_1 \\ i_2 \\ v_o \end{bmatrix}, \quad \tau = \frac{t}{\sqrt{L_1 C}} \tag{2}$$

where x_1, x_2 are the normalized input currents, x_3 is the normalized output voltage, and τ is the normalized time. Applying these relations to (1) yields

$$\frac{dx_1}{d\tau} = 1 - x_3 u_1 \tag{3a}$$

$$\theta_1 \frac{dx_2}{d\tau} = 1 - x_3 u_2 w_1 \tag{3b}$$

$$\frac{dx_3}{d\tau} = x_1 u_1 + \frac{x_2}{w_1} u_2 - \frac{x_3}{\theta_2} - \Delta_1 \tag{3c}$$

where

$$\theta_1 = \frac{L_2}{L_1}, \quad \theta_2 = R\sqrt{\frac{C}{L_1}}, \quad w_1 = \frac{v_1}{v_2}, \quad \Delta_1 = \frac{1}{v_1}\sqrt{\frac{L_1}{C}} i_L \tag{4}$$

and with the duty cycle logic complemented, we have

$$u_1 = 1 - \tilde{u}_1, \quad u_2 = 1 - \tilde{u}_2. \tag{5}$$

Note that the change of variable (2) has been adopted in previous studies (for example, see [28]–[31]) and is exploited in this paper to represent the parallel boost converters in a dimensionless form. Compared with the original model, this dimensionless representation features the following two main advantages: 1) The number of parameters is reduced from four (L_1, L_2, R, C) to only two (θ_1, θ_2), and 2) the number of exogenous inputs is decreased from three (v_1, v_2, i_L) to two (the ratio of input voltages w_1 and the normalized load current Δ_1). Hence, in the new coordinate system, the mathematical description of the converter is simplified, which, as we will see in the next section, facilitates the model analysis and controller design.

In the following section, we will work with the normalized model and assume that all the state variables are available to the controller, as well as the exogenous signals v_1 and v_2. Although this requirement implies the need for several sensors, in practice, the majority of these variables are available in the ESS, because, for the SOC calculation, the power flow in the energy sources, i.e., (v_1, i_1) and (v_2, i_2), must accurately be monitored.

III. DC-Link Controller

In this section, we present the dc-link control layer for the hybrid ESS structure illustrated in Fig. 1. It is assumed that the desired dc-bus voltage v_o^* and the SC current set point $i_2^* (= p_2^*/v_2)$ are specified by the VEM layer, e.g., using one of the methods mentioned in the Introduction, and are available to the lower control layers.

A. Control Problem

Given that the controller formulation will be based on the normalized model (3), it is appropriate to start the design by also normalizing the set points provided by the VEM layer. Accordingly, by applying the change of variable (2) to (v_o^*, i_2^*), we obtain the normalized references (x_2^*, x_3^*). After this preliminary step, the control objectives can be established as follows:

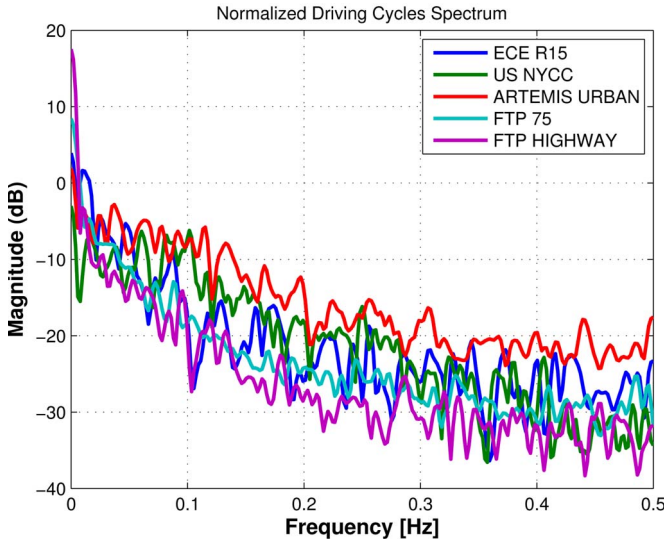

Fig. 3. Spectral density for some typical driving cycles.

Find a control law for (u_1, u_2) so that the converter outputs $\boldsymbol{y}$ follow the normalized set points, i.e.,

$$\mathbf{y}(\tau) = \begin{bmatrix} x_2(\tau) \\ x_3(\tau) \end{bmatrix} \rightarrow \begin{bmatrix} x_2^* \\ x_3^* \end{bmatrix} \tag{6}$$

as quickly as possible and being robust to uncertainties in the system (e.g., the powertrain load current).

Note that, in practice, (x_2^*, x_3^*) vary over time, depending on the vehicle state, driving cycle, and VEM algorithm. Consequently, from a theoretical perspective, the aforementioned regulation problem should be posed as an output-tracking problem. However, by following the tracking setting, it becomes necessary to find a stable inversion of the system [32], which is hampered by the nonlinearities and non-minimum-phase nature of the boost converter. In fact, the stable inverse of the boost model requires the inversion of the internal dynamics (in our case the battery current) that produces an Abel differential equation, which is difficult to analytically solve (see [31] and the references therein). To overcome these hurdles and under the assumption of slowly time-varying references (x_2^*, x_3^*), we will simplify the control problem by replacing the output-tracking setting by a regulation setting. The aforementioned assumption, which is perfectly reasonable for x_3^*, given that, the majority of the time, we aim at keeping a constant dc bus voltage, is more arguable in the case of the SC current set point x_2^*. Nevertheless, if we take into account the spectral distribution of the typical driving cycles to which the EV is subject, as depicted in Fig. 3, and even if x_2^* (or, equivalently, i_2^*) has to provide the high-frequency components, we can easily verify that the SC current/power will hardly contain a significant spectral content above 0.5 Hz. (This argument can also be extended to the disturbance Δ_1.) As a result, given the expected fast bandwidth of the dc-link controller, we can take (x_2^*, x_3^*) as slowly time-varying parameters, enabling the indirect solution of the tracking problem through a regulation setting.

In terms of nomenclature and for reasons that will later be clear, we will consider that the desired normalized output voltage $x_3^* = \theta_3$ is constant, whereas the variation of the SC current reference is bounded: $x_2^* = \Delta_2 \in [\underline{\Delta_2}, \overline{\Delta_2}] \subset \mathbb{R}$. Moreover, to cope with the inevitable parametric mismatch and nonmodeled factors, the controller will also incorporate integral action. Augmenting the normalized model (3) with an integral error, the converter can be represented by the following MIMO model:

$$\frac{d\boldsymbol{x}}{d\tau} = f(\boldsymbol{x}, \boldsymbol{u}, \boldsymbol{\theta}, w_1, \boldsymbol{\Delta}) = \begin{bmatrix} 1 - x_3 u_1 \\ (1 - x_3 u_2 w_1)/\theta_1 \\ x_1 u_1 + \frac{x_2}{w_1} u_2 - \frac{x_3}{\theta_2} - \Delta_1 \end{bmatrix} \tag{7a}$$

$$\frac{d\boldsymbol{\sigma}}{d\tau} = g(\boldsymbol{x}, \boldsymbol{\theta}, \boldsymbol{\Delta}) = \begin{bmatrix} x_2 - \Delta_2 \\ x_3 - \theta_3 \end{bmatrix} \tag{7b}$$

$$\mathbf{y} = \begin{bmatrix} x_2 & x_3 \end{bmatrix}^T \tag{7c}$$

where $\boldsymbol{x} = [x_1 \quad x_2 \quad x_3]^T$ and $\boldsymbol{\sigma} = [\sigma_1 \quad \sigma_2]^T$ are the states, $\boldsymbol{u} = [u_1 \quad u_2]^T \in [0,1] \times [0,1]$ is the control signal, and $\boldsymbol{\theta} = [\theta_1 \quad \theta_2 \quad \theta_3]^T$ are the model's constant parameters. The exogenous signal $w_1 \in \mathcal{D}_w \subset \mathbb{R}$ is known and belongs to the bounded set $\mathcal{D}_w$, which can be calculated by considering the expected voltage variation in the energy sources, e.g., $\mathcal{D}_w = [\underline{v_1}/\overline{v_2}, \overline{v_1}/\underline{v_2}]$. The bounded disturbance is described by $\boldsymbol{\Delta} = [\Delta_1 \quad \Delta_2]^T \in [\underline{\Delta_1}, \overline{\Delta_1}] \times [\underline{\Delta_2}, \overline{\Delta_2}] = \mathcal{D}_\Delta \subset \mathbb{R}^2$. Aside from the aforementioned considerations about the set points (x_2^*, x_3^*), the controller will further assume that the model parameters $\boldsymbol{\theta}$ are known and that $\boldsymbol{x}$, $\boldsymbol{\sigma}$ are available for feedback.

Our approach to the dc-link controller design will be based on a robust state-feedback control law. The first step of the design is to determine the equilibrium points of the nonlinear system (7) and perform the linearization around these points. Then, it will be shown that the resulting uncertain linear model lies in a convex polytope. This convex property will further be explored, starting from a robust LQR setting, to formulate an optimization problem with LMIs and extract the feedback gains. Finally, the operation range of the dc-link controller will be extended by gain scheduling the control gains with the exogenous signal w_1. Note that w_1, although unknown at the design stage, can be monitored during the system operation and, due to its slow variation, is a natural candidate for gain scheduling.

B. Control Law, Equilibrium Points, and Linearization

As a starting point for the dc-link controller design, suppose that the gain-scheduled variable $w_1 = \beta \in \mathcal{D}_w$ is constant (later, we will consider the time-varying case). With the aim of stabilizing (7), we propose a state feedback controller, which is expressed as

$$\boldsymbol{u} = \boldsymbol{K}_x(\beta)\boldsymbol{x} + \boldsymbol{K}_\sigma(\beta)\boldsymbol{\sigma} \tag{8}$$

where $\boldsymbol{K}_x(\beta) \in \mathbb{R}^{2\times 3}$ and $\boldsymbol{K}_\sigma(\beta) \in \mathbb{R}^{2\times 2}$ are the feedback gains. Under the reasonable assumption of nonsingular $\boldsymbol{K}_\sigma(\beta)$,

the family of equilibrium points of the MIMO system can be defined as

$$\begin{aligned}\boldsymbol{x}_{ss} &= \begin{bmatrix}\left(\frac{\theta_3^2}{\theta_2}+\theta_3\Delta_1-\frac{\Delta_2}{\beta^2}\right) & \Delta_2 & \theta_3\end{bmatrix}^T\\ \boldsymbol{u}_{ss} &= \begin{bmatrix}\frac{1}{\theta_3} & \frac{1}{\theta_3\beta}\end{bmatrix}^T\\ \boldsymbol{\sigma}_{ss} &= \left(\boldsymbol{K}_\sigma(\beta)\right)^{-1}\left(\boldsymbol{u}_{ss}-\boldsymbol{K}_x(\beta)\boldsymbol{x}_{ss}\right).\end{aligned} \tag{9}$$

Next, to investigate the local stability properties, the system (7) and (8) is linearized around the equilibrium point, resulting in the following state-space representation:

$$\frac{d\boldsymbol{x}_\delta}{d\tau} = \boldsymbol{A}\boldsymbol{x}_\delta + \boldsymbol{B}(\boldsymbol{\Delta})(\boldsymbol{K}_x\boldsymbol{x}_\delta + \boldsymbol{K}_\sigma\boldsymbol{\sigma}_\delta) \tag{10}$$

$$\frac{d\boldsymbol{\sigma}_\delta}{d\tau} = \boldsymbol{C}\boldsymbol{x}_\delta \tag{11}$$

where $\boldsymbol{x}_\delta = \boldsymbol{x}-\boldsymbol{x}_{ss}$, $\boldsymbol{\sigma}_\delta = \boldsymbol{\sigma}-\boldsymbol{\sigma}_{ss}$, $\boldsymbol{u}_\delta = \boldsymbol{u}-\boldsymbol{u}_{ss}$, and the matrices $\boldsymbol{A} = (\partial f/\partial \boldsymbol{x})$, $\boldsymbol{B}(\boldsymbol{\Delta}) = (\partial f/\partial \boldsymbol{u})$ and $\boldsymbol{C} = (\partial g/\partial \boldsymbol{x})$ are the Jacobians of the vector field, evaluated at the equilibrium point, and are given by

$$\begin{aligned}\boldsymbol{A} &= \frac{1}{\theta_3}\begin{bmatrix}0 & 0 & -1\\ 0 & 0 & -\frac{1}{\theta_1}\\ 1 & \frac{1}{\beta^2} & -\frac{\theta_3}{\theta_2}\end{bmatrix}\\ \boldsymbol{B}(\boldsymbol{\Delta}) &= \begin{bmatrix}-\theta_3 & 0\\ 0 & -\frac{\theta_3}{\theta_1}\beta\\ \boldsymbol{x}_{1ss}(\boldsymbol{\Delta}) & \frac{\Delta_2}{\beta}\end{bmatrix}\\ \boldsymbol{C} &= \begin{bmatrix}0 & 1 & 0\\ 0 & 0 & 1\end{bmatrix}.\end{aligned} \tag{12}$$

For ease of notation, the dependence of β in the feedback gains was dropped.

C. Polytopic Uncertainty

In the previous linear model, only the matrix $\boldsymbol{B}$ is affected by the disturbance $\boldsymbol{\Delta}$, which, for convenience, can be rewritten as

$$\boldsymbol{B}(\boldsymbol{\Delta}) = \underbrace{\begin{bmatrix}-\theta_3 & 0\\ 0 & -\frac{\theta_3}{\theta_1}\beta\\ 0 & 0\end{bmatrix}}_{\boldsymbol{B}_0} + \underbrace{\begin{bmatrix}0 & 0\\ 0 & 0\\ 1 & 0\end{bmatrix}}_{\boldsymbol{B}_a}\boldsymbol{x}_{1ss}(\boldsymbol{\Delta}) + \underbrace{\begin{bmatrix}0 & 0\\ 0 & 0\\ 0 & \frac{1}{\beta}\end{bmatrix}}_{\boldsymbol{B}_b}\Delta_2 \tag{13}$$

where $x_{1ss}(\boldsymbol{\Delta})$ represents the battery current at the equilibrium (the first element of $\boldsymbol{x}_{ss}$). Note that this relation displays an affine form in the variables x_{1ss} and Δ_2. This fact, together with the bounds

$$x_{1ss}(\boldsymbol{\Delta}) \in [\underline{x}_1, \overline{x}_1], \qquad \Delta_2 \in [\underline{\Delta}_2, \overline{\Delta}_2] \tag{14}$$

where $\underline{x}_1$, $\overline{x}_1$ can easily be extracted from $\mathcal{D}_\Delta$, $\mathcal{D}_w$, enables us to represent the uncertainty of the linear model in the following convex polytope, which is composed of four vertices:

$$\begin{aligned}[\boldsymbol{A} \quad \boldsymbol{B}(\boldsymbol{\Delta})] \in \operatorname{co}\{&[\boldsymbol{A} \quad (\boldsymbol{B}_0+\boldsymbol{B}_a\underline{x}_1+\boldsymbol{B}_b\underline{\Delta}_2)]\\ &[\boldsymbol{A} \quad (\boldsymbol{B}_0+\boldsymbol{B}_a\underline{x}_1+\boldsymbol{B}_b\overline{\Delta}_2)]\\ &[\boldsymbol{A} \quad (\boldsymbol{B}_0+\boldsymbol{B}_a\overline{x}_1+\boldsymbol{B}_b\underline{\Delta}_2)]\\ &[\boldsymbol{A} \quad (\boldsymbol{B}_0+\boldsymbol{B}_a\overline{x}_1+\boldsymbol{B}_b\overline{\Delta}_2)]\}.\end{aligned} \tag{15}$$

The aforementioned well-known convex-hull operator [33] $\operatorname{co}\{.\}$ is given by

$$[\boldsymbol{A} \quad \boldsymbol{B}(\boldsymbol{\Delta})] \in \left\{\sum_{i=1}^{L}\lambda_i[\boldsymbol{A}_i \quad \boldsymbol{B}_i]: \quad \lambda_i \geq 0, \sum_{i=1}^{L}\lambda_i = 1\right\} \tag{16}$$

where $[\boldsymbol{A}_i \quad \boldsymbol{B}_i]$ represents vertices of the polytope, as defined in (15), and $L = 4$.

D. Control Synthesis

After the derivation of the linearized uncertain model, in this section, we will explain how the state feedback matrices $(\boldsymbol{K}_x, \boldsymbol{K}_\sigma)$ can be selected to obtain a stable and robust controller. With this goal in mind, let us consider the augmented state $\boldsymbol{\xi}_\delta = [\boldsymbol{x}_\delta \quad \boldsymbol{\sigma}_\delta]^T$ and its dynamics, i.e.,

$$\frac{d\boldsymbol{\xi}_\delta}{d\tau} = \underbrace{\begin{bmatrix}\boldsymbol{A} & 0\\ \boldsymbol{C} & 0\end{bmatrix}}_{\mathcal{A}}\boldsymbol{\xi}_\delta + \underbrace{\begin{bmatrix}\boldsymbol{B}(\boldsymbol{\Delta})\\ 0\end{bmatrix}}_{\mathcal{B}(\boldsymbol{\Delta})}\underbrace{\begin{bmatrix}\boldsymbol{K}_x & \boldsymbol{K}_\sigma\end{bmatrix}}_{\mathcal{K}}\boldsymbol{\xi}_\delta \tag{17a}$$

$$= \left(\mathcal{A}+\mathcal{B}(\boldsymbol{\Delta})\mathcal{K}\right)\boldsymbol{\xi}_\delta. \tag{17b}$$

Following the discussion carried out in the previous section, the augmented state and input matrix $(\mathcal{A}, \mathcal{B}(\boldsymbol{\Delta}))$, which are assumed to form a controllable pair in $\boldsymbol{\Delta} \in \mathcal{D}_\Delta$, are contained in the following convex polytope:

$$\begin{aligned}[\mathcal{A} \quad \mathcal{B}(\boldsymbol{\Delta})] \in \operatorname{co}\{&[\mathcal{A}_1 \quad \mathcal{B}_1], [\mathcal{A}_2 \quad \mathcal{B}_2]\\ &[\mathcal{A}_3 \quad \mathcal{B}_3], [\mathcal{A}_4 \quad \mathcal{B}_4]\}\end{aligned} \tag{18}$$

where $\mathcal{A}_i$, $\mathcal{B}_i$, $i = 1, \ldots, L$ follow from (15) and (17).

In simple terms, the first robust stability problem that we need to solve can be stated as follows: find the state feedback gains $\mathcal{K}$ such that $(\mathcal{A}+\mathcal{B}(\boldsymbol{\Delta})\mathcal{K})$ is Hurwitz for any $\boldsymbol{\Delta} \in \mathcal{D}_\Delta$. To address this problem, we can apply the Lyapunov method and pose an LMI problem that is solvable by numerical means (see [33, Ch. 7]). However, this formulation neglects a very important aspect, i.e., the transient response of the closed-loop system is not taken into account in the control synthesis. Thus, to ensure a satisfactory transient performance, in addition to robustness, we will seek the minimization of the following quadratic cost function:

$$J = \int_0^\infty \boldsymbol{\xi}_\delta(s)^T(\boldsymbol{Q}+\mathcal{K}^T\boldsymbol{R}\mathcal{K})\boldsymbol{\xi}_\delta(s)ds \tag{19}$$

where $\boldsymbol{Q} = \boldsymbol{Q}^T > 0$, $\boldsymbol{R} = \boldsymbol{R}^T > 0$ are positive-definite symmetric matrices defined by the designer. Toward the robust minimization of J (which can be regarded as a robust LQR problem), consider a quadratic Lyapunov candidate function, $V = \boldsymbol{\xi}_\delta^T\boldsymbol{P}\boldsymbol{\xi}_\delta$, with $\boldsymbol{P} = \boldsymbol{P}^T > 0$, as well as its time derivative, as

$$\dot{V} = \boldsymbol{\xi}_\delta^T\left(\left(\mathcal{A}+\mathcal{B}(\boldsymbol{\Delta})\mathcal{K}\right)^T\boldsymbol{P} + \boldsymbol{P}\left(\mathcal{A}+\mathcal{B}(\boldsymbol{\Delta})\mathcal{K}\right)\right)\boldsymbol{\xi}_\delta. \tag{20}$$

Spurred by the guaranteed-cost control concept [34], suppose that a pair $(\mathcal{K}, \boldsymbol{P})$ can be chosen such that the following inequality is satisfied:

$$\dot{V} = \boldsymbol{\xi}_\delta^T \left((\mathcal{A} + \mathcal{B}(\boldsymbol{\Delta})\mathcal{K})^T \boldsymbol{P} + \boldsymbol{P} (\mathcal{A} + \mathcal{B}(\boldsymbol{\Delta})\mathcal{K}) \right) \boldsymbol{\xi}_\delta < -\boldsymbol{\xi}_\delta^T (\mathbf{Q} + \mathcal{K}^T \mathbf{R} \mathcal{K}) \boldsymbol{\xi}_\delta \quad (21)$$

for any $\boldsymbol{\Delta} \in \mathcal{D}_\Delta$. Because $\boldsymbol{Q}$, $\boldsymbol{R} > 0$, it follows that $\boldsymbol{Q} + \mathcal{K}^T \boldsymbol{R} \mathcal{K} > 0$, $\dot{V} < 0$ $\forall \boldsymbol{\xi}_\delta \neq 0$ and asymptotic stability is obtained [35]. Next, integrating the previous relation

$$\int_0^\infty \dot{V}(s) ds = V(\infty) - V(0) < -\int_0^\infty \boldsymbol{\xi}_\delta^T (\mathbf{Q} + \mathcal{K}^T \mathbf{R} \mathcal{K}) \boldsymbol{\xi}_\delta ds \quad (22)$$

and using the asymptotic stability property, i.e., $V(\infty) \to 0$, we have

$$J < V(0) = \boldsymbol{\xi}_\delta(0)^T \boldsymbol{P} \boldsymbol{\xi}_\delta(0). \quad (23)$$

Hence, the cost J can be bounded by the initial value of the Lyapunov function, which also depends on the initial state $\boldsymbol{\xi}_\delta(0)$. To eliminate this dependence, we can consider a stochastic interpretation of (23), as suggested in [36] and [37], and take $\boldsymbol{\xi}_\delta(0)$ as a random vector with zero mean and covariance equal to the identity matrix. Applying the expected value operator to the resulting random variable, $\mathbb{E}\{\boldsymbol{\xi}_\delta(0)^T \boldsymbol{P} \boldsymbol{\xi}_\delta(0)\}$, a new upper bound, independent of $\boldsymbol{\xi}_\delta(0)$, is obtained as [36]

$$J < \text{trace}(\mathbf{P}). \quad (24)$$

Returning to the inequality (21), it can be shown that, by exploring the convexity property of the uncertain polytope, (21) holds if the following matrix inequalities are true:

$$(\mathcal{A}_i + \mathcal{B}_i \mathcal{K})^T \boldsymbol{P} + \boldsymbol{P} (\mathcal{A}_i + \mathcal{B}_i \mathcal{K}) + \mathbf{Q} + \mathcal{K}^T \boldsymbol{R} \mathcal{K} < 0 \quad (25)$$

for $i = 1, \ldots, L$. This result, together with (24), enables us to recast the robust optimization problem as

$$\min_{\mathcal{K}, \boldsymbol{P}} \quad \text{trace}(\boldsymbol{P}) \quad s.t. \quad \boldsymbol{P} > 0, \quad (25), \quad i = 1, \ldots, L. \quad (26)$$

At this stage, note that the formulation (26) intends to minimize the upper bound on the cost function J. This approach is known in the literature as the guaranteed-cost control [34], [36] and ensures that the resulting controller will provide an adequate level of performance in spite of uncertainties in the model. The main obstacles to the numerical resolution of (26) are the nonconvex constraints. To overcome this difficulty, we apply the following change of variable (as suggested in [33]):

$$\boldsymbol{Y} = \boldsymbol{P}^{-1}, \qquad \boldsymbol{L} = \mathcal{K} \boldsymbol{Y} \quad (27)$$

which, after some algebraic manipulation, allows us to reformulate the robust stabilization problem in a more practical setting:

Proposition 1: Consider the model (17), under polytopic uncertainty (18). The guaranteed-cost control problem as defined in (26) is equivalent to

$$\min_{\boldsymbol{L}, \boldsymbol{Y}} \quad -\text{trace}(\boldsymbol{Y}) \quad s.t. \quad \begin{bmatrix} -\boldsymbol{Y} \mathcal{A}_i^T - \mathcal{A}_i \boldsymbol{Y} - \mathcal{B}_i \boldsymbol{L} - \boldsymbol{L}^T \mathcal{B}_i^T & \boldsymbol{Y} & \boldsymbol{L}^T \\ \boldsymbol{Y} & \boldsymbol{Q}^{-1} & 0 \\ \boldsymbol{L} & 0 & \boldsymbol{R}^{-1} \end{bmatrix} > 0 \quad \boldsymbol{Y} > 0, i = 1, \ldots, L \quad (28)$$

where $\mathcal{K} = [\boldsymbol{K}_x \quad \boldsymbol{K}_\sigma] = \boldsymbol{L} \boldsymbol{Y}^{-1}$.

Note that, in this last formulation, the constraints are placed as LMIs, which are convex and easier to treat numerically. In fact, the YALMIP [38] and SeDuMi solvers [39] were employed to numerically extract the optimal solution of the aforementioned problem.

E. Gain Scheduling

So far, we have assumed that the exogenous input $w_1 = v_1/v_2$ is constant, but in practice, this variable depends on the voltage of the energy sources, which varies over the EV operation. To deal with this variation and extend the operation range of the dc-link controller, the feedback gains $\boldsymbol{K}_x$, $\boldsymbol{K}_\sigma$ will be modified (scheduled) according to the value of w_1 (the scheduled variable). Toward that aim, we start by discretizing the exogenous input w_1 over its domain $(\mathcal{D}_w)$ as

$$[\beta_1, \beta_2, \ldots, \beta_N] \in (\mathcal{D}_w)^N \subset \mathbb{R}^N. \quad (29)$$

Next, for each one of these discrete values, we apply (28) to calculate (offline) the corresponding set of control gains as

$$(\boldsymbol{K}_x(\beta_1), \boldsymbol{K}_\sigma(\beta_1)), \ldots, (\boldsymbol{K}_x(\beta_N), \boldsymbol{K}_\sigma(\beta_N)). \quad (30)$$

The gain-scheduled controller is then obtained by replacing β (constant) with w_1 (slowly time varying) in (8) and interpolating the controller gains at intermediate points, producing the final control law, i.e.,

$$\boldsymbol{u} = \boldsymbol{K}_x(w_1) \boldsymbol{x} + \boldsymbol{K}_\sigma(w_1) \boldsymbol{\sigma} \quad (31)$$

which is illustrated in Fig. 4. To qualitatively analyze the influence of scheduled variable w_1 in the feedback gains, Fig. 5 represents the (linear) interpolation results of $\boldsymbol{K}_x(w_1)$ and $\boldsymbol{K}_\sigma(w_1)$ used in the experimental validation (whose details will be discussed in the next section). Based on these results, it is interesting to note that some feedback gains are almost insensitive to w_1 variations, e.g., the x_2 feedback gain in the u_1 channel, whereas other feedback gains show the opposite behavior (e.g., the x_3 feedback gain in the u_1 channel depicts a variation of more than 300% throughout the w_1 operation range). Furthermore, note that the dimensionless model (3) adopted in the dc-link controller design brings important advantages to the gain-scheduling implementation. To be more precise, instead of using two scheduled variables (v_1 and v_2), as would be the case if the original model (1) was employed in

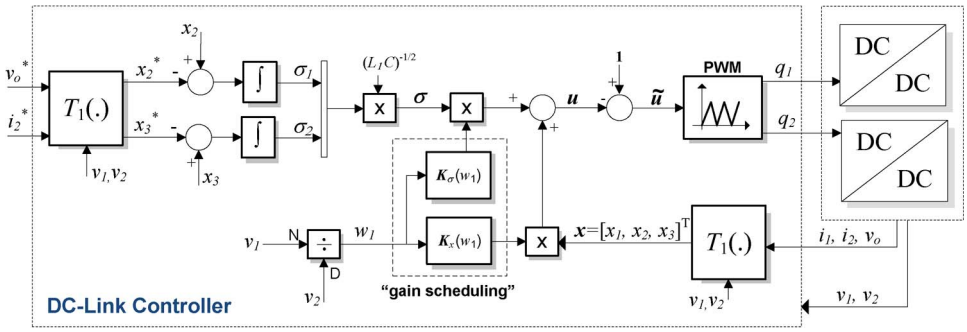

Fig. 4. Block diagram of the proposed dc-link controller. Note that the change of variable $T_1(.)$ is described by (2).

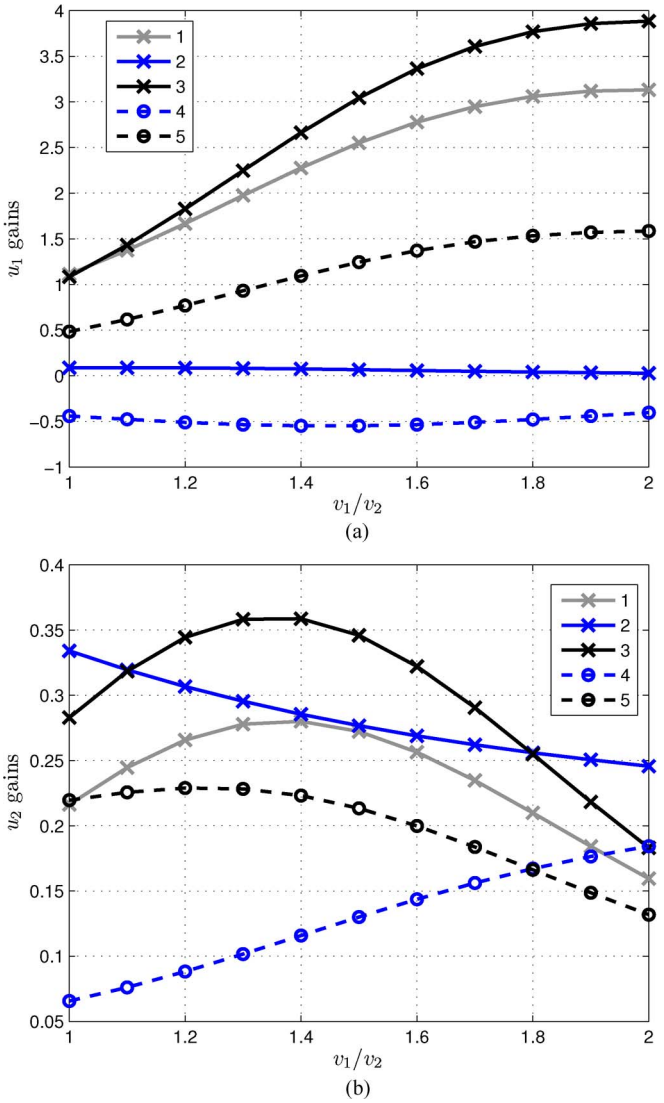

Fig. 5. Feedback gains of the gain-scheduled dc-link controller (31) employed in the experimental validation. The u_1 gains represent the first row of the matrix $[\boldsymbol{K}_x(w_1)\ \boldsymbol{K}_\sigma(w_1)]$, whereas the u_2 gains represent the second row. (a) u_1 gains. (b) u_2 gains.

the controller design, the approach proposed in this paper needs only a single variable, i.e., the voltage ratio w_1.

Remark 1: To ensure that the gain-scheduling controller (31) maintains the stability and transient response performance, it is necessary that the exogenous input varies slowly in time [40]. To show that this requirement holds in our design, recall the definition $w_1 = v_1/v_2$ and notice that the time variation of the battery voltage v_1, compared with the high excursion that is usually observed in v_2, can safely be neglected. In other words, v_2 is definitely the variable that contributes most to the variation of w_1. Hence, using the SC ideal model, the evolution of v_2 can be described by

$$v_2(t) = v_2(0) + \frac{1}{C_{SC}} \int_0^t i_2(s)ds \tag{32}$$

where C_{SC} is the equivalent capacitance of the SCs. Because C_{SC} is normally chosen with a relatively high value, the integral relation (32) provides a slow variation in v_2. Consequently, taking into account the time scale that the dc-link controller operates (some milliseconds), it is perfectly reasonably to admit w_1 as slowly varying exogenous input.

Remark 2: In this paper, it was considered that the dc-link voltage must remain constant throughout the EV operation, which may be conservative for some designs. For example, the dc-bus voltage increase can be helpful when the load power is high [41] or during the field-weakening operation of the electric motor [42]. Nonetheless, the design described here can easily be extended to deal with variable x_3^*, e.g., by adding a second gain-scheduling variable (x_3^*) to the controller.

From a practical point of view, implementing the control law (31), particularly the integral action, requires certain care on a number of details. First, note that the controller was formulated in normalized time (τ), whereas its implementation will be done in normal time (t); therefore, it is imperative to introduce a correction factor when integrating the regulation error, i.e.,

$$\frac{d\boldsymbol{\sigma}}{dt} = \frac{1}{\sqrt{L_1 C}} \frac{d\boldsymbol{\sigma}}{d\tau}. \tag{33}$$

Second, to avoid unwanted transients upon the controller activation, the initial value of the integrator $\boldsymbol{\sigma}(0)$ should be selected, taking into account the initial conditions (i.e., $\boldsymbol{x}(0)$, $w_1(0)$) and the intended initial duty cycles $\boldsymbol{u}(0)$. Based on this information, we can invert (31) and extract an adequate value for $\boldsymbol{\sigma}(0)$. Finally, because the control signals are physically limited, it is essential to incorporate antiwindup mechanisms into the integrators to ensure proper operation when $\boldsymbol{u}$ saturates. With this concern in mind, we employed the technique of the conditional integrator [43].

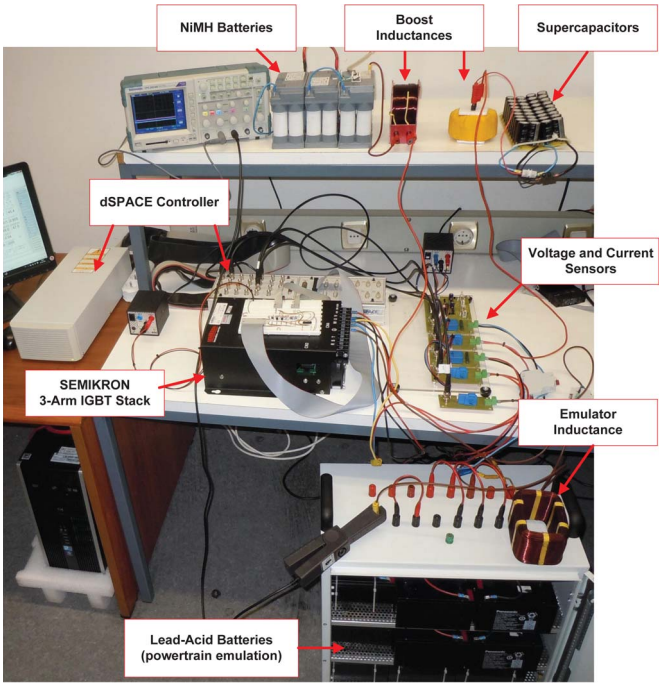

Fig. 6. Experimental test bench employed in the dc-link controller validation.

TABLE I
PARAMETERS OF THE EXPERIMENTAL TEST BENCH

Parameter	Value
L_1	10 mH
L_2	5 mH
C	1 mF
R	250Ω
v_1	$[47\ 52]V$
v_2	$[26\ 48]V$

IV. EXPERIMENTAL VALIDATION

A. Overview of the Experimental Setup

The experimental validation of the dc-link controller was carried out in a small laboratory test bench, built with the intention of studying, in a reduced power scale (1:70), the hybrid ESS of the EV prototype VEIL [44], [45]. This reduced-scale setup (dc link with 500 W and 100 V), as illustrated in Fig. 6, is endowed with the following two types of energy sources: 1) a battery pack and 2) a SCs bank. The battery pack is composed of four NiMH Saft modules (12 V and 13.5 Ah) [46] in series, whereas the SCs bank is obtained by two branches of SCs in parallel of a series of 18 cells (100 F, 2.7 V, and 21.4 A), which was manufactured by NESSCAP [47]. Each energy source is connected to the dc link through a bidirectional boost converter, whose power electronics were accomplished by two (of the three) arms of the SEMIKRON–SKS 11F B6CI (600 V/18 A) module, switched at 10 kHz. The remaining arm of the power module is used to build a third bidirecional boost converter, with the objective of emulating the (reduced) powertrain load that is requested to the dc link. Table I describes the parametric values employed in the experimental setup.

With regard to the dc-link controller implementation, a dSPACE DS1103 real-time card was employed and programmed through the MATLAB–Simulink–RTW environment. The voltage and current measurements, accomplished through Hall-effect transducers, LEM LV25-P and HY15-P, respectively, are acquired by the analog-to-digital converters of the dSPACE board, in synchrony with the PWM signals.

Before the final implementation, the performance, robustness, and gain-scheduling parameters of the dc-link controller must be chosen. The performance parameters were taken as

$$\boldsymbol{R} = \text{diag}\,([1 \quad 1]), \quad \boldsymbol{Q} = 1.10^{-2}\text{diag}\,([1 \quad 1 \quad 1 \quad 5 \quad 5]) \tag{34}$$

where diag(.) is the diagonal matrix. With regard to the robustness parameters, associated with the uncertainty bounds, they were defined as $x_{1ss}(\boldsymbol{\Delta}) \in [-0.7, 0.7]$, $\Delta_2 \in [-0.5, 0.5]$, which is equivalent to a variation of ± 11 A in the battery current and ± 8 A in the SCs and is enough to cover the power range of the experimental tests. Furthermore, taking into account the expected range for v_1 and v_2 voltages, as defined in Table I, it was assumed that the gain-scheduled variable $w_1 = v_1/v_2$ belongs to the set [1, 2]. Then, w_1 was discretized with a fixed step size of 0.1, generating a grid with $N = 11$ points $(\beta_1, \beta_2, \ldots, \beta_N)$, and for each one of these, (28) was solved with the YALMIP+SeDuMi solver, producing a family of controllers described in (30). The final implementation of the LQR robust-gain-scheduling (LQR-R-GS) controller in the dSPACE was carried out through lookup tables, which were used to store the family of feedback gains (30) and by interpolating them for intermediate results (see Fig. 5). Although the lookup tables must store 110 points and perform 10 interpolations in each sampling time, the complexity of this operation is moderately low, because all the tables share the same input, which enables the application of efficient prelookup techniques [48].

As control objectives, it is required that the LQR-R-GS keeps the output voltage constant at $v_o^* = 100$ V and ensures that the SC current tracks a given time-varying reference i_2^*.

B. Evaluation of the Robust Formulation

The first batch of experimental tests intends to assess the benefits of designing the dc-link controller within a robust framework. To that purpose, the LQR-R-GS was compared to a nominal LQR controller, called LQR-N, which does not take into account any kind of uncertainty in the model and assumes constant exogenous inputs. In other words, the LQR-N has fixed Δ_1, Δ_2, and w_1. Given that the EV operating conditions significantly change through time, one difficulty that emerges when implementing the nominal controller is the selection of the operating point. To address this problem, we employed the average operating point of the system, which, for our purposes here, was taken as $(x_{1ss}, x_{2ss}, w_1) = (0.4, 0.2, 1.042)$ or, in nonnormalized variables, $(i_{1ss}, i_{2ss}, v_1/v_2) = (6.32\text{ A}, 3.16\text{ A}, 50\text{ V}/48\text{ V})$. Moreover, the LQR-N gains were obtained by solving (19) with the MATLAB *lqr* command, and for a fair comparison, both controllers share the same performance

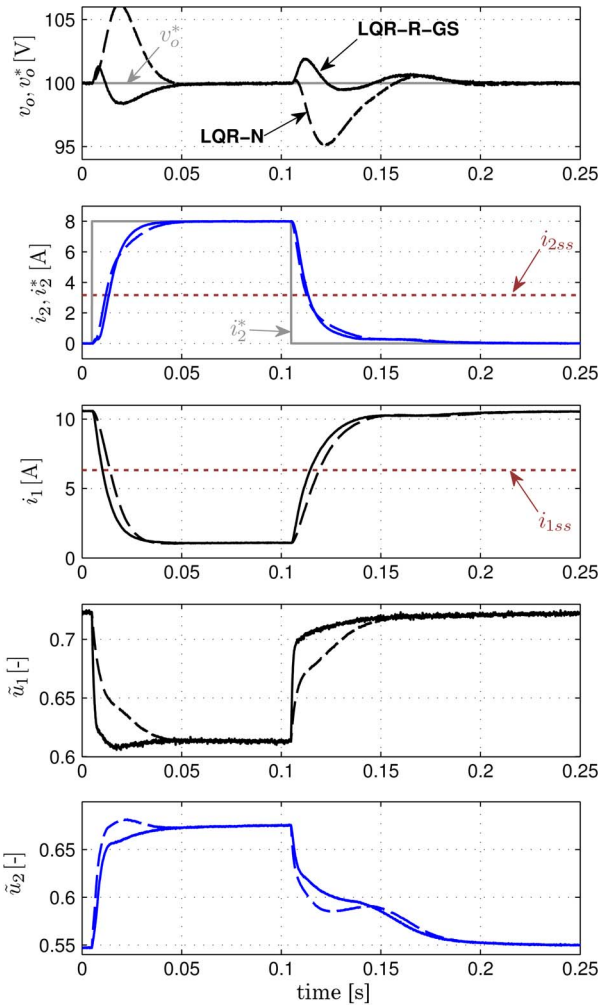

Fig. 7. Experimental results of the LQR-R-GS (full line) and nominal LQR (dashed line) controllers when excited with a step in i_2^*. The nominal point employed in the nominal LQR tuning is $(i_{1ss}, i_{2ss}) = (6.32\text{ A}, 3.16\text{ A})$ (dotted line), and the remaining exogenous inputs/disturbances are kept constant $(i_L = 4.0\text{ A}, w_1 = 50\text{ V}/48\text{ V})$.

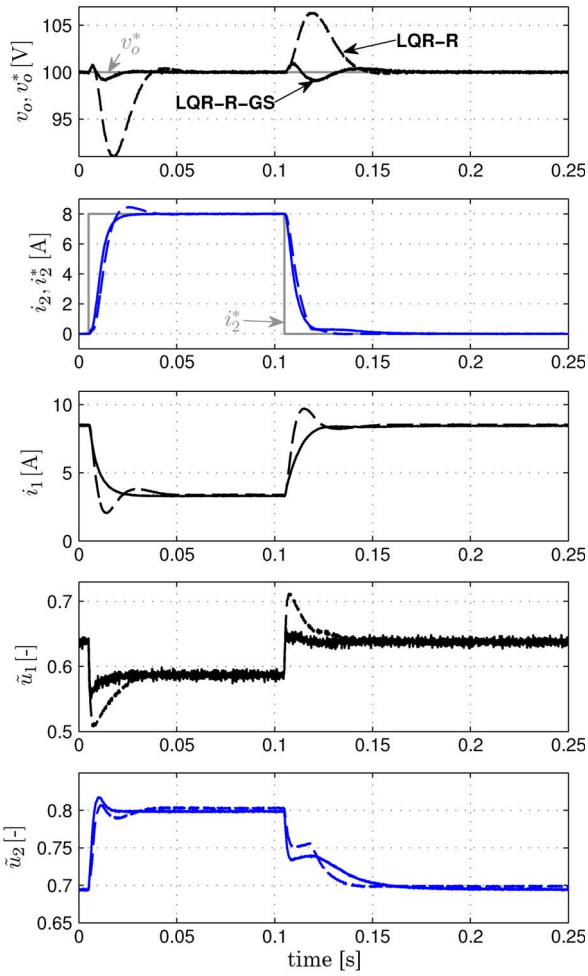

Fig. 8. Experimental results of the LQR-R-GS (full line) and robust LQR without gain scheduling (dashed line) controllers when excited with a step in i_2^*. The SC voltage approaches the full discharge $(w_1 = 50\text{ V}/32\text{ V})$ but remains approximately constant throughout the test, as well as the load current $i_L = 3.5$ A. LQR-R (without gain scheduling) was configured, assuming fully charged SCs.

weights, as defined in (34). The resulting nominal controller is defined as

$$\boldsymbol{K}_{LQR-N} = [\,\boldsymbol{K}_{x,N} \quad \boldsymbol{K}_{\sigma,N}\,] = \begin{bmatrix} -0.457 & -0.031 & -0.268 & 0.125 & -0.185 \\ -0.036 & -0.331 & -0.005 & -0.185 & -0.126 \end{bmatrix}. \quad (35)$$

As far as i_2^* is concerned, during the first experimental test, a small pulse (100 ms and 8 A of peak) is applied to the SC reference, maintaining the other exogenous inputs/disturbances (w_1, i_L) constant. Analyzing the experimental results depicted in Fig. 7, we can find that the LQR-R-GS offers a superior transient performance in regulating the output voltage, reducing the peak voltage errors from 6% (LQR-N) to less than 2%, whereas a small improvement is obtained in the i_2^* tracking. Some of these differences can be explained by looking more closely at the control signals evolution, i.e., the duty cycles $(\tilde{u}_1, \tilde{u}_2)$. For example, the results show that the nominal controller is much faster in modifying the duty cycle of the SCs u_2 than u_1. As a consequence, during the initial positive step $(t \in [0.01, 0.11]\text{ s})$, the batteries are slower in terms of coming out of service (and the SCs are too quick in terms of supplying the power), which leads to excess energy being injected in the dc bus. This energy, in turn, is absorbed by the dc-link capacitor, producing a considerable voltage overshoot that is present with the LQR-N controller (a dual case occurs at $t \in [0.11, 0.25]$ s, where the battery reentry in service is also slow, leading to the voltage undershoot). From a theoretical point of view, the transient performance deterioration that is shown in the LQR-N was, to some extent, expected because the controller moves around the nominal point employed in its tuning (see i_{1ss} and i_{2ss} as plotted in Fig. 7). On the other hand, the LQR-R-GS design takes into account the uncertainty in the operating conditions and provides better coordination among the sources. It is also worth mentioning that, due to the integral action, no differences are found between controllers in the steady state.

C. Evaluation of the Gain Scheduling

After establishing the benefits of the robust formulation, we will now assess the impact of gain scheduling the dc-link controller with the input voltages ratio $(w_1 = v_1/v_2)$.

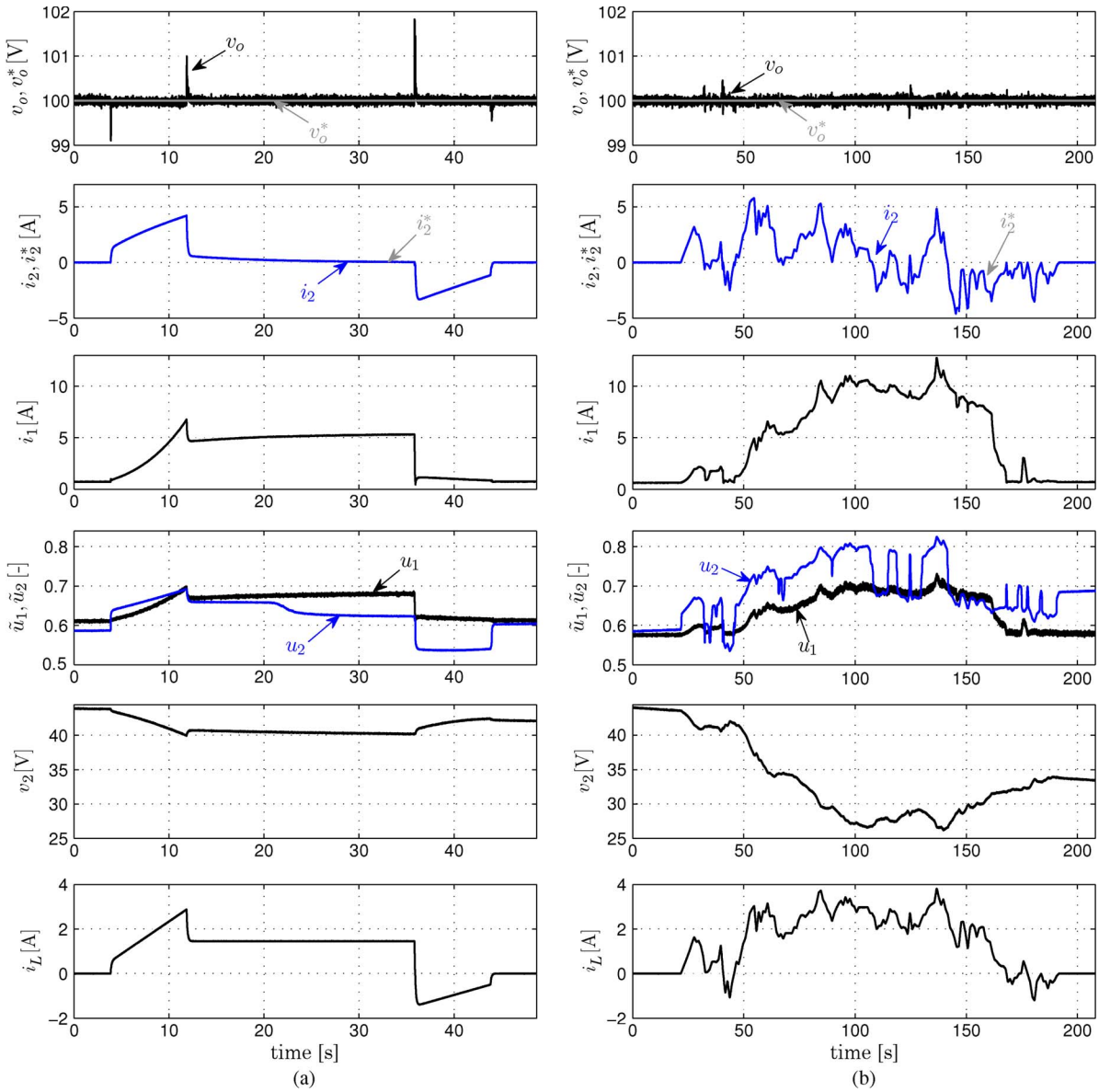

Fig. 9. Experimental results for some selected driving cycles. The high-pass filter (36), which was responsible for generating i_2^*, was configured with $\tau_f = 8$ s (manual cycle) and $\tau_f = 15$ s (FTP75 cycle). (a) Manual cycle, which comprises standstill, accelerating, cruising, and decelerating operation modes. (b) FTP75 driving cycle (136–351 s).

To investigate this issue, the LQR-R-GS will be compared with the robust LQR without gain scheduling, i.e., assuming a constant exogenous input $w_1 = \beta_e$. This latter controller, referred to as LQR-R, is characterized by a state feedback with the structure $\boldsymbol{K}_{LQR-R} = [\boldsymbol{K}_{x,R} \quad \boldsymbol{K}_{\sigma,R}]$, where the fixed gains are extracted based on Fig. 5, i.e., $\boldsymbol{K}_{x,R} = \boldsymbol{K}_x(\beta_e)$, $\boldsymbol{K}_{\sigma,R} = \boldsymbol{K}_\sigma(\beta_e)$. With regard to the experiments conducted in this section, the LQR-R was configured by assuming a fully charged SC ($\beta_e = 50$ V/48 V) and evaluated for the case where the SC is close to the discharge point ($v_1/v_2 = 50$ V/32 V). The remaining conditions are similar to the ones used in the previous test.

The experimental results, as shown in Fig. 8, demonstrate a superior transient performance of the LQR-R-GS against the LQR-R, i.e., the voltage regulation error for the gain-scheduling controller is less than 2%, contrasting with the 8% peak error for the LQR-R, whereas minor differences are observed in the SC current tracking. Further insight can be gained by analyzing these results from a power-flow perspective. The nonscheduled controller is configured under the assumption that the SCs are fully charged with 48 V; thus, when the 8-A step is applied to i_2^*, the LQR-R takes for granted that the SC will supply $48 \times 8 = 384$ W (the model did not consider losses) and, as result, reduces the battery power in the same proportion. However, in practice, the SC has a lower voltage, i.e., 32 V, resulting in power delivery of only $32 \times 8 = 256$ W, i.e., much less than was expected. Meanwhile, the power reduction conducted in the battery is still done under the assumption of fully charged SCs, which generates a power shortage in the dc link, driving to the voltage undershoot that occurs with the LQR-R controller around $t \in [0.01 \ 0.05]$ s (a dual situation happens at $t \in [0.11 \ 0.15]$ s, but with an inverse consequence, i.e., excessive power in the dc link). In fact, to recover the voltage stability, the LQR-R must rely on an integral action to eliminate

the parametric mismatch, which leads to the observed transient degradation. On the other hand, the scheduled controller greatly benefits from adapting the gains according to the exogenous input, producing a much better power shift among the energy sources and reducing the power imbalances during transients.

D. Evaluation With Driving Cycles

In the previous sections, the experimental tests primarily focused on assessing the local transient performance of the LQR-R-GS for a limited set of operating points. In this section, we will move on to a global evaluation, covering a wider range of operating conditions and concentrating on a more realistic setting, based on driving cycles. To that aim, the load emulator was configured to take, from the dc link, a given amount of power in accordance with some predefined cycles. Of the various driving cycles that were experimentally evaluated, two of them were selected and shown here. First, a manual cycle, composed of 8 s of acceleration, 25 s of cruising at constant speed, and 8 s of deceleration (plus 8 s of standstill) was built and applied to the experimental setup [see Fig. 9(a)]. Second, a rescaled FTP75 cycle was tested, of which the results for the period between 136 and 341 s are presented in Fig. 9(b). A second important modification that was carried out in these latter tests concerns the generation of the SCs' current/power set points, which is the responsibility of the VEM layer (see Fig. 1). Accordingly, the SCs' current reference was generated using a frequency-based power allocation, which is mathematically defined as a high-pass filter, i.e.,

$$i_2^* = \frac{\tau_f s}{\tau_f s + 1} \frac{p_L}{v_2} \tag{36}$$

where s is the Laplace operator, τ_f is the time constant of the filter, and p_L is the power requested by the vehicle. This filter-based power split, which has been discussed in the literature [20], [49], [50], is motivated by the idea of using the SCs to satisfy the high-frequency content of the dc-link power p_L, whereas the average power is provided by the batteries. Although the VEM algorithm is not the main subject of this paper, (36) represents a simple and practical way of generating the SC set point i_2^* and enables us to validate the LQR-R-GS controller in a more realistic setting.

Fig. 9(a) and (b) depicts the final experimental results for the aforementioned driving cycles. In both cases, the dc-link output voltage v_o is accurately regulated, presenting maximum voltage errors below 2% in the manual cycle and 0.5% in the FTP75. Similarly, the tracking of the SC current displays negligible errors and, for time scales under consideration, i_2^* is almost overlapped with the measured current i_2. The FTP75 test also enables us to investigate the LQR-R-GS performance when subject to a considerable excursions in the SC voltage, which greatly affects the gain-scheduling variable $w_1 = v_1/v_2$. Despite facing a 50% variation in v_2 throughout the FTP75 test, the LQR-R-GS controller schedules its gains according to these variations and can keep a uniform performance in the dc-link control task, independent of the SC state of charge. Finally, Fig. 10 depicts the power sharing between the sources throughout the FTP75 cycle. Analyzing these results, we can find that the batteries supply the average power requested by the EV load (p_L), whereas the SCs cover the acceleration transients and high-frequency content, which are in accordance with the expected behavior for the frequency-based power splitting employed in the VEM layer.

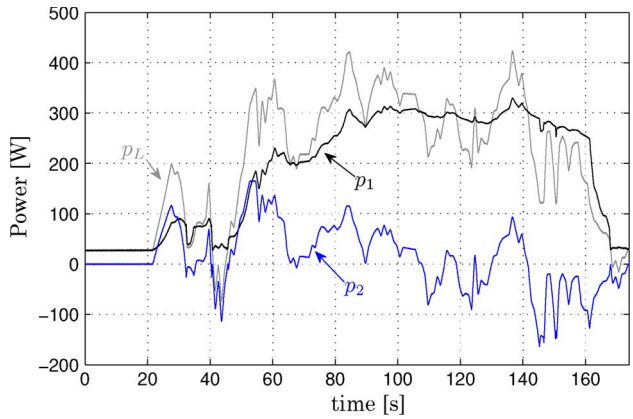

Fig. 10. Experimental results of the power provided by the battery ($p_1 = v_1 i_1$) and SCs ($p_2 = v_2 i_2$) and requested by the load ($p_L = (i_L + (v_o/R))v_o$) during the tests depicted in Fig. 9. (a) FTP75 driving cycle (136–351 s).

V. Conclusion

In this paper, a robust dc-link controller for the hybridization of batteries and SCs, through an active parallel topology composed of two bidirectional boost dc–dc converters, has been presented. The proposed approach relies on an LQR framework and can simultaneously control, in a coordinated manner, the dc bus voltage and the SC current. This LQR setting was then extended to deal with the following two important issues in the dc-link layer: 1) model uncertainty and 2) exogenous disturbances. With regard to model uncertainty, we notice that a convex uncertain model can be built for the power converters, enabling us to translate the robust LQR into an LMI-based optimization problem, which is easily solvable by numerical means. To handle the issue of exogenous disturbances, the controller was gain scheduled with the energy sources' voltages, which, in view of the SCs' voltage variations, proved to be very effective. The implementation of the gain-scheduling technique also greatly benefited from the dimensionless representation of the dc–dc converters, which enabled us to handle the effect of the two energy sources voltages in the dc-link controller using only a single scheduled variable, i.e., the ratio $w_1 = v_1/v_2$. Experimental validation, which was carried out in a reduced-scale test bench, demonstrated the effectiveness of the proposed dc-link controller. In particular, it was shown that, compared with two other methods (a nominal LQR and a robust LQR without gain scheduling), the proposed controller offers better transient response, especially in the dc-bus regulation task. Additional experimental evaluation with realistic driving cycles (FTP75) was also provided, confirming a satisfactory performance of the dc-link controller when subject to a wider range of operation conditions.

As future work, we intend to validate the dc-link controller in one of our full-scale EV prototypes and address the VEM layer.

ACKNOWLEDGMENT

The authors would like to thank M. Miranda for his help in setting up the power converter of the experimental test bench.

REFERENCES

[1] C. C. Chan, A. Bouscayrol, and K. Chen, "Electric, hybrid, and fuel-cell vehicles: Architectures and modeling," *IEEE Trans. Veh. Technol.*, vol. 59, no. 2, pp. 589–598, Feb. 2010.

[2] A. Khaligh and Z. Li, "Battery, ultracapacitor, fuel cell, and hybrid energy storage systems for electric, hybrid electric, fuel cell, and plug-in hybrid electric vehicles: State of the art," *IEEE Trans. Veh. Technol.*, vol. 59, no. 6, pp. 2806–2814, Jul. 2010.

[3] S. Vazquez, S. M. Lukic, E. Galvan, L. G. Franquelo, and J. M. Carrasco, "Energy storage systems for transport and grid applications," *IEEE Trans. Ind. Electron.*, vol. 57, no. 12, pp. 3881–3895, Dec. 2010.

[4] S. M. Lukic, C. Jian, R. C. Bansal, F. Rodriguez, and A. Emadi, "Energy storage systems for automotive applications," *IEEE Trans. Ind. Electron.*, vol. 55, no. 6, pp. 2258–2267, Jun. 2008.

[5] A. de Guibert, "Batteries and supercapacitor cells for the fully electric vehicle," in *Proc. Smart Syst. Integr. Conf.*, Brussels, Belgium, 2009.

[6] P. G. Pereirinha and J. P. Trovão, "Comparative study of multiple energy sources utilization in a small electric vehicle," in *Proc. 3rd Eur. Ele-Drive Transp. Conf.*, Geneva, Switzerland, 2008.

[7] M. B. Camara, H. Gualous, F. Gustin, and A. Berthon, "Design and new control of DC/DC converters to share energy between supercapacitors and batteries in hybrid vehicles," *IEEE Trans. Veh. Technol.*, vol. 57, no. 5, pp. 2721–2735, Sep. 2008.

[8] P. Thounthong, V. Chunkag, P. Sethakul, B. Davat, and M. Hinaje, "Comparative study of fuel-cell vehicle hybridization with battery or supercapacitor storage device," *IEEE Trans. Veh. Technol.*, vol. 58, no. 8, pp. 3892–3904, Oct. 2009.

[9] M. B. Camara, H. Gualous, F. Gustin, A. Berthon, and B. Dakyo, "DC/DC converter design for supercapacitor and battery power management in hybrid vehicle applications-polynomial control strategy," *IEEE Trans. Ind. Electron.*, vol. 57, no. 2, pp. 587–597, Feb. 2010.

[10] M. Ortuzar, J. Moreno, and J. Dixon, "Ultracapacitor-based auxiliary energy system for an electric vehicle: Implementation and evaluation," *IEEE Trans. Ind. Electron.*, vol. 54, no. 4, pp. 2147–2156, Aug. 2007.

[11] J. Dixon, I. Nakashima, E. F. Arcos, and M. Ortuzar, "Electric vehicle using a combination of ultracapacitors and ZEBRA battery," *IEEE Trans. Ind. Electron.*, vol. 57, no. 3, pp. 943–949, Mar. 2010.

[12] Z. Li, O. Onar, A. Khaligh, and E. Schaltz, "Design, control, and power management of a battery/ultracapacitor hybrid system for small electric vehicles," presented at the Soc. Autom. Eng., World Congr. Exh., Detroit, MI, 2009, SAE Paper 2009-01-1387.

[13] L. Solero, A. Lidozzi, and J. A. Pomilio, "Design of multiple-input power converter for hybrid vehicles," *IEEE Trans. Power Electron.*, vol. 20, no. 5, pp. 1007–1016, Sep. 2005.

[14] A. A. Ferreira, J. A. Pomilio, G. Spiazzi, and L. de Araujo Silva, "Energy management fuzzy logic supervisory for electric vehicle power supplies system," *IEEE Trans. Power Electron.*, vol. 23, no. 1, pp. 107–115, Jan. 2008.

[15] R. de Castro, P. Melo, P. Pacheco, R. E. Araujo, and D. Freitas, "A control allocation approach to manage multiple energy sources in EVs," in *Proc. IEEE VPPC*, Chicago, IL, 2011, pp. 1–6.

[16] O. Sundstrom, D. Ambuhl, and L. Guzzella, "On implementation of dynamic programming for optimal control problems with final state constraints," *Oil Gas Sci. Technol.—Rev. IFP*, vol. 65, no. 1, pp. 91–102, Jan./Feb. 2010.

[17] A. Sciarretta and L. Guzzella, "Control of hybrid electric vehicles," *IEEE Control Syst.*, vol. 27, no. 2, pp. 60–70, Apr. 2007.

[18] C. Romaus, K. Gathmann, and J. Böcker, "Optimal energy management for a hybrid energy storage system for EVs based on stochastic dynamic programming," in *Proc. IEEE Veh. Power Propulsion Conf.*, 2010, pp. 1–6.

[19] J. Moreno, M. E. Ortuzar, and J. W. Dixon, "Energy-management system for a hybrid electric vehicle, using ultracapacitors and neural networks," *IEEE Trans. Ind. Electron.*, vol. 53, no. 2, pp. 614–623, Apr. 2006.

[20] A. L. Allegre, A. Bouscayrol, and R. Trigui, "Influence of control strategies on battery/supercapacitor hybrid energy storage systems for traction applications," in *Proc. IEEE VPPC*, Dearborn, MI, 2009, pp. 213–220.

[21] R. de Castro, J. P. Trovão, P. Pacheco, P. Melo, P. G. Pereirinha, and R. E. Araujo, "DC link control for multiple energy sources in electric vehicles," in *Proc. IEEE VPPC*, Chicago, IL, 2011, pp. 1–6.

[22] R. Erickson and D. Maksimović, *Fundamentals of Power Electronics*, 2nd ed. Norwell, MA: Kluwer, 2001.

[23] C. Olalla, R. Leyva, A. El Aroudi, and I. Queinnec, "Robust LQR control for PWM converters: An LMI approach," *IEEE Trans. Ind. Electron.*, vol. 56, no. 7, pp. 2548–2558, Jul. 2009.

[24] C. Olalla, R. Leyva, A. El Aroudi, P. Garces, and I. Queinnec, "LMI robust control design for boost PWM converters," *IET Power Electron.*, vol. 3, no. 1, pp. 75–85, Jan. 2010.

[25] C. Olalla Martinez, I. Queinnec, R. Leyva, and A. El Aroudi, "Optimal state-feedback control of bilinear DC–DC converters with guaranteed regions of stability," *IEEE Trans. Ind. Electron.*, vol. 59, no. 10, pp. 3868–3880, Oct. 2012.

[26] C. Olalla, I. Queinnec, R. Leyva, and A. El Aroudi, "Robust optimal control of bilinear DC–DC converters," *Control Eng. Pract.*, vol. 19, no. 7, pp. 688–699, Jul. 2011.

[27] D. Maksimovic, A. M. Stankovic, V. J. Thottuvelil, and G. C. Verghese, "Modeling and simulation of power electronic converters," *Proc. IEEE*, vol. 89, no. 6, pp. 898–912, Jun. 2001.

[28] H. Sira-Ramírez, "On the generalized PI sliding mode control of DC-to-DC power converters: A tutorial," *Int. J. Control*, vol. 76, no. 9/10, pp. 1018–1033, Jun. 2003.

[29] H. Sira-Ramírez and R. Silva-Ortigoza, *Control Design Techniques in Power Electronics Devices*. New York: Springer-Verlag, 2006.

[30] C. Albea, F. Gordillo, and C. Canudas-de Wit, "Adaptive control design for a boost inverter," *Control Eng. Pract.*, vol. 19, no. 1, pp. 32–44, Jan. 2011.

[31] J. M. Olm, X. Ros-Oton, and Y. B. Shtessel, "Stable inversion of Abel equations: Application to tracking control in DC–DC nonminimum phase boost converters," *Automatica*, vol. 47, no. 1, pp. 221–226, Jan. 2011.

[32] S. Devasia, C. Degang, and B. Paden, "Nonlinear inversion-based output tracking," *IEEE Trans. Autom. Control*, vol. 41, no. 7, pp. 930–942, Jul. 1996.

[33] S. Boyd, L. El Ghaoui, E. Feron, and V. Balakrishnan, *Linear Matrix Inequalities in System and Control Theory*. Philadelphia, PA: SIAM, 1994.

[34] S. Chang and T. Peng, "Adaptive guaranteed cost control of systems with uncertain parameters," *IEEE Trans. Autom. Control*, vol. AC-17, no. 4, pp. 474–483, Aug. 1972.

[35] H. Khalil, *Nonlinear Systems*, 3rd ed. Englewood Cliffs, NJ: Prentice-Hall, 2002.

[36] I. R. Petersen and D. C. McFarlane, "Optimal guaranteed cost control and filtering for uncertain linear systems," *IEEE Trans. Autom. Control*, vol. 39, no. 9, pp. 1971–1977, Sep. 1994.

[37] S. Tarbouriech, G. Garcia, J. da Silva, and I. Queinnec, *Stability and Stabilization of Linear Systems With Saturating Actuators*. New York: Springer-Verlag, 2011.

[38] J. Lofberg, "Modeling and solving uncertain optimization problems in YALMIP," in *Proc. 17th IFAC World Congr.*, Seoul, Korea, 2008.

[39] J. F. Sturm, "Using SeDuMi 1.02, A MATLAB toolbox for optimization over symmetric cones," *Optim. Methods Softw.*, vol. 11/12, no. 1–4, pp. 625–653, 1999.

[40] W. J. Rugh and J. S. Shamma, "Research on gain scheduling," *Automatica*, vol. 36, no. 10, pp. 1401–1425, Oct. 2000.

[41] E. Rask, M. Duoba, and H. Lohse-Busch, "Recent hybrid electric vehicle trends and technologies," in *Proc. IEEE VPPC*, Chicago, IL, 2011, pp. 1–6.

[42] K. Yamamoto, K. Shinohara, and T. Nagahama, "Characteristics of permanent-magnet synchronous motor driven by PWM inverter with voltage booster," *IEEE Trans. Ind. Appl.*, vol. 40, no. 4, pp. 1145–1152, Jul./Aug. 2004.

[43] A. Visioli, *Practical PID Control*. New York: Springer-Verlag, 2006.

[44] J. P. Trovão, P. G. Pereirinha, and H. M. Jorge, "Analysis of operation modes for a neighborhood electric vehicle with power sources hybridization," in *Proc. IEEE Veh. Power Propulsion Conf.*, 2010, pp. 1–6.

[45] J. P. Trovão, P. G. Pereirinha, and H. M. Jorge, "Design methodology of energy storage systems for a small electric vehicle," *World Elect. Veh. J.*, vol. 3, pp. 1–12, 2009.

[46] *Smart VH Module Datasheet*, Saft, Bagnolet, France.

[47] *NESSCAP Ultracapacitor Datasheet (ESHSR-0100C0-002R7)*, NESSCAP, Toronto, ON, Canada, 2003.

[48] Mathworks, Natick, MA, Prelookup Block Module Documentation, 2011.

[49] T. Azib, O. Bethoux, G. Remy, C. Marchand, and E. Berthelot, "An innovative control strategy of a single converter for hybrid fuel cell/supercapacitor power source," *IEEE Trans. Ind. Electron.*, vol. 57, no. 12, pp. 4024–4031, Dec. 2010.

[50] T. Azib, O. Bethoux, G. Remy, and C. Marchand, "Saturation management of a controlled fuel-cell/ultracapacitor hybrid vehicle," *IEEE Trans. Veh. Technol.*, vol. 60, no. 9, pp. 4127–4138, Nov. 2011.
[51] R. de Castro, R. E. Araujo, and H. Oliveira, "Design, development and characterization of a FPGA platform for multimotor electric vehicle control," in *Proc. 5th IEEE Veh. Power Propulsion Conf.*, Dearborn, MI, 2009, pp. 145–152.

Ricardo de Castro (S'09) was born in Porto, Portugal, in 1983. He received the *Licenciatura* degree in electrical and computer engineering from the University of Porto in 2006. He is currently working toward the Ph.D. degree with the Department of Electrical and Computer Engineering, Faculty of Engineering, University of Porto.

From 2007 to 2008, he was an Entrepreneur with the WeMoveU Project, targeting the development of powertrain control solutions for light electric vehicles. His research interests include active safety systems for electric vehicles, tire–road friction estimation, and battery–supercapacitor hybridization.

Rui Esteves Araújo (M'99) was born in Viana do Castelo, Portugal, in 1964. He received the B.Sc. degree in electrical engineering and the M.Sc. and Ph.D. degrees from the University of Porto, Porto, Portugal, in 1987, 1992, and 2001, respectively.

From 1987 to 1988, he was an Electrotechnical Engineer with the Project Department, Adira Company, Porto. From 1988 to 1989, he was Researcher with the Institute for Systems and Computer Engineering of Porto (INESC Porto; now INESC TEC). Since 1989, he has been with the University of Porto, where he is currently an Assistant Professor with the Department of Electrical and Computer Engineering, Faculty of Engineering, University of Porto. Since April 2010, he has been a Researcher with the Power Systems Unit, INESC TEC. He is also currently a Consultant with the European Commission Framework Programmes and has coordinated two national research projects. He has published more than 50 technical papers and is the holder of one patent. His teaching interests include power electronics, electrical machines, and drives. His contributions are focused on field motion control for industrial, electrical vehicular, and automotive applications. His research interests include energy efficiency in electric machines, the design and control of power converters, industrial electronics applications to distributed power generation systems based on renewable energies, and motion control applied to electric vehicles.

João Pedro F. Trovão (S'08) was born in Coimbra, Portugal, in 1975. He received the Electrical Engineering and M.Sc. degrees (Power Systems branch) in 1999 and 2004, respectively, from the University of Coimbra, where is currently working toward the Ph.D. degree.

Since 2000, he has been a Teaching Assistant with the Department of Electrical Engineering, Polytechnic Institute of Coimbra–Coimbra Institute of Engineering (IPC–ISEC). Since 2007, he has been a Researcher with the Institute for Systems and Computers Engineering at Coimbra (INESC Coimbra). His research interests include electric vehicles, renewable energy, energy management, power quality, and rotating electrical machines.

Mr. Trovão received the 2006 Best Technical Paper Award for a paper that was published in the Portuguese and Brazilian peer-reviewed journal *Manutenção*.

Paulo G. Pereirinha (S'04–M'06) received the Ph.D. degree in electrical engineering from the University of Coimbra, Coimbra, Portugal.

Since 1995, he has been with the Polytechnic Institute of Coimbra–Coimbra Institute of Engineering (IPC–ISEC), where he is currently a Coordinator Professor with the Department of Electrical Engineering and the President of the Scientific Committee. His classes and research interests include electrical machines, electric vehicles, electromechanical drives, finite elements, and renewable energies.

Dr. Pereirinha is a Founding Member of the Portuguese Electric Vehicle Association (APVE) and a member of the APVE Administration Board, the Portuguese Electrotechnical Normalization Technical Committees CTE 69—Electric Systems for Electric Road Vehicles and CT 146—Electric Road Vehicles, and the Portuguese Engineers Order.

Pedro Melo (S'10) received the B.Sc. degree in electrical engineering and the M.Sc. degree from the University of Porto, Porto, Portugal, where he is currently working toward the Ph.D. degree.

Since 2001, he has been with the Department of Electrical Engineering, School of Engineering, Polytechnic Institute of Porto, as an Assistant Professor. His research interests include electrical machine modelling and control, the design and materials for high-efficiency machines, and energy management systems for electric vehicles.

Diamantino Freitas was born in Porto, Portugal, in 1954. He received the B.Sc. degree in electrotechnical engineering and the Ph.D. degree (with a focus on the modeling of electroacoustic transfer functions) from the University of Porto in 1991 and in 1976, respectively.

In 1974, he was a Teaching Assistant with the Department of Electrical and Computer Engineering, Faculty of Engineering, University of Porto, where he has been an Associate Professor since 2003. He has participated and coordinated several research and development (R&D) projects and was a national delegate to several European COST Actions, for example, COST 288 and COST 219. Since 2003, he has done regular consultancy in electroacoustics for the Fatima Shrine, Portugal. Since 2005, he has been the Technical Leader of the NAVMETRO system for the guidance of blind persons with the metro transport system of Porto. Over the past 10 years, he has been the author or a coauthor of 82 papers that have been published in international conference proceedings with reviewers, seven international book chapters, and 13 papers in international journals. He is the holder of one national patent. His research interests include applications of signal processing, particularly electroacoustics, system identification and modeling, automatic speech processing, accessibility for persons with special needs, biomedical engineering, and rehabilitation.